Wind and Structures, *Vol. 28, No. 5 (2019) 331-345*
DOI: https://doi.org/10.12989/was.2019.28.5.331

Influence of geometric configuration on aerodynamics of streamlined bridge deck by unsteady RANS

Md. N. Haque[*1,2], Hiroshi Katsuchi[2a], Hitoshi Yamada[2b] and Haeyoung Kim[2c]

[1]*Department of Civil Engineering, East West University, A/2 Jahurul Islam Avenue, Jahurul Islam City, Aftabnagar, Dhaka-1212, Bangladesh*
[2]*Department of Civil Engineering, Yokohama National University, 79-1, Tokiwadai, Hodogaya-ku, Yokohama 240-8501, Japan*

(Received February 16, 2017, Revised February 26, 2019, Accepted March 11, 2019)

Abstract. Long-span bridge decks are often shaped as streamlined to improve the aerodynamic performance of the deck. There are a number of important shaping parameters for a streamlined bridge deck. Their effects on aerodynamics should be well understood for shaping the bridge deck efficiently and for facilitating the bridge deck design procedure. This study examined the effect of various shaping parameters such as the bottom plate slope, width ratio and side ratio on aerodynamic responses of single box streamlined bridge decks by employing unsteady RANS simulation. Steady state responses and flow field were analyzed in detail for wide range of bottom plate slopes, width and side ratios. Then for a particular deck shape Reynolds number effect was investigated by varying its value from $1.65x10^4$ to $25x10^4$. The aerodynamic response showed very high sensitivity to the considered shaping parameters and exhibited high aerodynamic performance for a particular combination of shaping parameters.

Keywords: streamlined bridge deck; bottom plate slope; width ratio; aerodynamic force coefficients; flow field; pressure distribution; Reynolds number; Side ratio; CFD and unsteady RANS

1. Introduction

Aerodynamic stability of long-span cable-supported bridge decks is one of the important design criteria both from serviceability and critical state points of view. As the span length of the bridge increases the deck becomes flexible in nature which makes them vulnerable against wind effects. A number of bridges have shown wind induced vibration (Fujino and Siringoringo 2013). The shape of the bridge deck plays an important role to improve the aerodynamic responses. Therefore, the aerodynamics of the bridge deck should be well understood to maximize the aerodynamic performance that can be achieved by shaping the bridge decks to avoid expensive post construction countermeasures.

Various shapes have already been adopted for long-span bridges; one of most popular and widely applied shape is the single box streamlined bridge deck as shown in Fig.1. A number of long-span bridges have adopted this kind of shape such as Great Belt Bridge, Nanjin-4 Bridge, Sutong Bridge, Incheon Bridge, Osteroy Bridge, Tsurumi Tsubasa Bridge and many others. The streamlined shape is achieved by means of making the bottom plate of the girder inclined and adding a small fairing at both sides of the deck.

Many researches have already been dedicated regarding this kind of shape. Yamaguchi *et al*. (1986) against vortex-induced vibration and flutter instability. They found that shape of the fairing influences the aerodynamic response and recommended further investigation. Then, Nagao *et al*. (1993), Kawatani *et al.* (1993), Sakai *et al.* (1993), Larsen (1993), De Miranda and Bartoli (2001), Sukamta *et al.* (2008), Haque *et al.* (2014) and Haque *et al.* (2016) investigated the influence of fairings on aerodynamic response. They also found that fairing has effectiveness to improve mean force coefficients, vortex shedding behavior and flutter wind speed. However, discussion was limited to its effectiveness only without any systematic and detailed investigation to understand the influence of shaping parameters.

Then, Larsen and Wall (2012) conducted wind tunnel investigation on a streamlined deck to know the influence and the optimum slope of the bottom plate to facilitate the bridge deck shaping procedure, as this is one of the common shaping parameters that is adjusted to improve the aerodynamic performance of this kind of deck. They considered three bottom plate slopes (θ_B) of 25°, 20° and 14.8° and compared their free vibration responses. They recommended a θ_B of 14.8° to eliminate vortex-induced vibration as the vortex forms away from the bridge deck. Before that, Wang *et al.* (2009) also dedicated detailed wind tunnel investigation to select the deck shape for Nanjing 4th Bridge having various θ_B to improve the flutter wind speed. They found that the flutter wind speed increases dramatically for a θ_B of less than 16°. On the other hand, Haque *et al.* (2015a, b) devoted an elaborate numerical

*Corresponding author, Ph.D.
E-mail: naimul@ewubd.edu
[a] Professor
E-mail: katsuchi@ynu.ac.jp
[b] Professor
E-mail: y-yamada@ynu.ac.jp
[c] Ph.D.
E-mail: kimhy@ynu.ac.jp

ISSN: 1226-6116 (Print), 1598-6225 (Online)

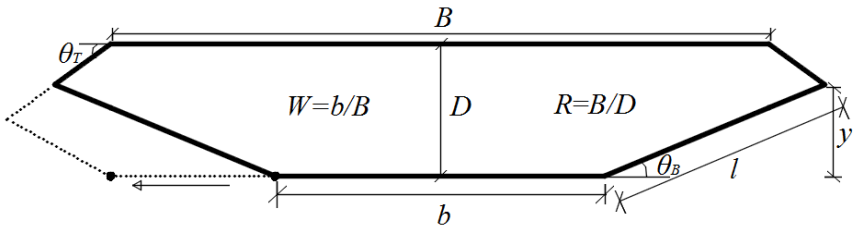

Fig. 1 A typical streamlined bridge deck and important notations

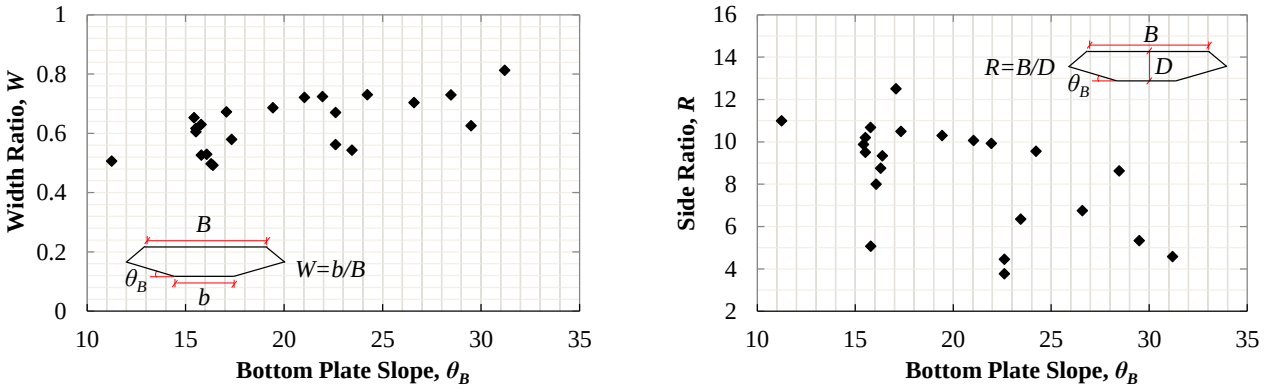

Fig. 2 Geometric properties of existing streamlined bridge decks. Data were collected from various research articles and websites of the construction and consulting companies

study for a pentagonal shape bridge deck. They investigated the influence of number of shaping parameters such curb angle and curb height including the bottom plate slope of the pentagonal bridge deck. The bottom plate slope was varied from 10° t o16°. Due the pentagonal shape, the bridge deck did not have any bottom plate horizontal width (b). The optimum aerodynamic responses were obtained for the bottom plate slope of around 11°. Later, Haque et al. (2016) conducted another detailed study on a bridge deck with edge fairing where the θ_B of the edge faring was altered between 10°-40°. The bridge decks with edge fairing had a b equal to the width of top plate (B) of the bridge. For bridge deck with edge fairing, the optimum aerodynamic responses shifted to higher value of θ_B which is near about 20°.

Hence, for streamlined bridge deck (as shown in Fig. 1), the θ_B may not be an independent shaping parameter to optimize the aerodynamic responses. The orientation of θ_B may depend on a number of other parameters such as the top plate slope (θ_T), b and the side ratio (R=B/D) of the bridge deck. For the same value of θ_B, the orientation varies significantly in terms of nose location (y) and the length of the inclined bottom plate (l) when any of these parameters are changed keeping the others same. Further, for existing bridges the preliminary shape and some of the dimensions such as the width (B, b) and the height (D) of the deck are determined based on the traffic volume, structural, architectural, maintenance points of view. Improvement of the aerodynamic response by adjusting the θ_B is required to be done in a secondary stage for a given set of dimensions. Therefore, knowing the influence of θ_B on aerodynamic responses in relation to the other parameters is quite an important issue as this can help the designer to take the prompt decision for shaping the bridge deck aerodynamically.

To make the representation simpler, we define a new shaping parameter named width ratio (W=b/B). For a given value of θ_T and R, if the W alters the orientation of bottom plate slope will also alter as shown in Fig. 1. We surveyed the detailed section geometries of 22 long-span cable-supported bridge decks such as the Great Belt Bridge (Denmark), Nanjing-4 Bridge (China), Incheon Bridge (Korea), Ostorey Bridge (Norway), Tsurumi Tsubasa Bridge (Japan) etc. and found that the W varies noticeably from 0.7 to 0.5 as shown in Fig. 2. Even, the width ratio (W) can be as high as 1 for the bridge deck with edge fairing such as Bronx-whitestone (USA), Hakucho (Japan) and Tempozan (Japan) Bridges etc. Therefore, the influence of W on aerodynamics of bridge deck is obvious as it varies within a wide range of value for existing bridges. Similar to the W, the θ_B and R also vary quite well from 11° to 30° and from 5° to 13°, respectively.

Another important aspect is that in past works (Wang *et al.* 2009 and Larsen and Wall 2012) only the vibration amplitudes at various wind speeds were focused, yet the flow field was not explored in detail to understand the influence of those shaping parameters. In addition, the steady state response such as drag force, lift force and moment coefficients is also important and should be treated equally to the dynamic responses as they are basic

parameters resulting from the flow field around the deck. Influence of shaping parameters (θ_B, W and R) on steady state force coefficients should be well known and the Reynolds number (R_e) effect is also required to be considered. Further, the past works were limited to wind tunnel study only. No detailed numerical work has been dedicated to reconfirm the outcomes of the experimental works and to improve further understanding about the aerodynamics of bridge deck by exploring flow field numerically.

Taking all these issues into consideration, in the present work a detailed and systematic numerical investigation was carried out for single box streamlined bridge decks by employing unsteady RANS to clarify the influence of various shaping parameters on its aerodynamic response and flow field. First, the influence of θ_B, W and R on steady state force coefficients were investigated at a particular Reynolds number (R_{eB}, was normalized by the deck width B) of $6.0\text{x}10^4$. The W was varied from 0.3 to 1 and for each of this W, θ_B was varied from 11° to 25°. Two different values of R viz. 5 and 8 were utilized for the same set of θ_B and W to understand the influence of R. The pressure, velocity and vorticity fields were analyzed in detail to apprehend the trend obtained in the force coefficients. The R_{eB} effects on steady state response and flow field were also explored by varying the value from $1.65\text{x}10^4$ to $25\text{x}10^4$.

2. Governing equation and numerical setup

The flow around the bridge deck was assumed as two-dimensional and incompressible in nature. Ensemble averaged unsteady Reynolds-Averaged Navier-Stokes (URANS) equations were used to simulate the flow around the deck. The governing equations are as follows

$$\frac{\partial \overline{U}_i}{\partial x_i} = 0 \tag{1}$$

$$\frac{\partial \overline{U}_i}{\partial t} + \overline{U}_j \frac{\partial \overline{U}_i}{\partial x_j} = -\frac{1}{\rho}\frac{\partial \overline{P}}{\partial x_i} + \frac{\partial}{\partial x_j}\left[\nu\left(\frac{\partial \overline{U}_i}{\partial x_j} + \frac{\partial \overline{U}_j}{\partial x_i}\right) - (\overline{u_i' u_j'})\right] \tag{2}$$

where $\overline{U}_i$ is the mean velocity vector, x_i is the position vector, t is time, $\overline{P}$ is the averaged pressure, ρ is the air density, ν is the kinematic viscosity of the fluid. Due to time averaging process, the new variable $\overline{u_j' u_i'}$ appears. It is the fluctuating component of the flow and demands modeling to close the equation. It is known as turbulence modeling.

Turbulence modeling was attained by the k-ω-SST model (Menter 1993, Menter and Esch 2001). This turbulence model has superiority over the other popular models as it grasps the advantages of both the k-ε and k-ω turbulence models. Further a number of applications (Šarkić *et al*. 2012, Brusiani *et al.* 2013, Miranda *et al*. 2014, Nieto *et al.* 2015, Patruno 2015) of this model can be found in bridge aerodynamics field.

The governing equations were discretized by Finite Volume Method (FVM) and an open source code OpenFOAM was used as a solver. A second-order accurate bounded total variational diminishing (TVD) scheme resulting from the application of a limiter function to the central differencing was utilized to discretize the convective terms. The Diffusive terms were approximated by central-differencing scheme of second-order accuracy. Time advancement was achieved by the implicit two-step second order backward differentiation formulae (BDF) method. For static simulation the pressure-velocity coupling was attained by Pressure-implicit PISO algorithm with a predictor-corrector approach. To maintain stability of the simulations the maximum Courant number (C_o) was maintained well below 1.

The domain size and meshing are shown in Fig. 3. The domain size was selected based on past researches and recommendations (Kelkar and Patankar 1992, Sohankar *et al.* 1995, Sohankar *et al.* 1998, Franke *et al.* 2004). The domain was sufficiently large to avoid unnecessary disturbance of the boundary conditions. A non-slip boundary condition ($\partial u/\partial y \neq 0$ and $v = 0$) was imposed on the bridge deck. A Dirichlet type boundary condition for velocity ($u = U$ and $v = 0$) and Neumann type boundary condition for pressure ($\partial p/\partial n = 0$) were implemented at the inlet of the domain while Neumann type for velocity and Dirichlet type for pressure were applied at the outlet of the domain. A slip boundary condition ($\partial u/\partial y = 0$ and $v = 0$) was imposed at the top and bottom of the domain.

A body fitted structured grid system was utilized to discretized the flow spatially as shown in Fig. 4. In previous studies (Haque *et al.* 2015b, c, 2016), we carried out detailed grid dependency test for bluff bodies along with a sharp-edged bridge deck section and the same grid system was adopted for the present study. Fist grid height (y) normal to deck section was tried to select such that it remains in the viscous sub-layer ($y^+ \leq 5$) and the grids were stretched gradually away from the deck surface in all directions. In general, the bridge deck had an average y^+ value ($y^+ = \rho y u^*/\mu$ where u^* is the friction velocity and μ is the dynamic viscosity) of 2.3 around the periphery of bridge deck with a maximum and minimum y^+ values of 0.2 and 7, respectively. At a very small area near the top surface leading edge corner the maximum value of y^+ appeared and except that, in all other location around the bridge deck boundary the y^+ value was well below 5 as indicated by the averaged value (Avg. $y^+ = 2.3$). Similar bound of y^+ value was also utilized by Šarkić *et al.* (2012). In the present study mainly, relative comparison was made among the aerodynamic responses of various deck shapes, hence, the similarity of grid system in terms of y^+ value is one of the main issues to make the comparison valid. Giving priority to that issue, in all the simulations almost similar bound (variation of y^+ was around 5%) of y^+ value was maintained regardless of variation of shape and R_{eB}. When R_{eB} was altered, the first grid height was also adjusted accordingly to maintain similar range of y^+ value. Therefore, at high R_{eB} ($\geq 13\text{x}10^4$) the simulation became both spatially and temporally expensive.

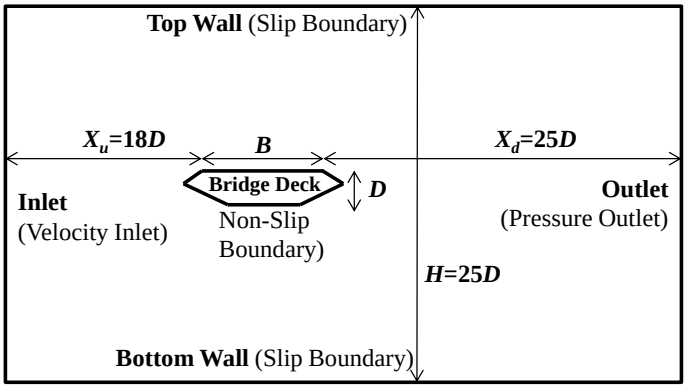

Fig. 3 Domain size and the boundary conditions adopted in the present study for simulating flow around the bridge deck

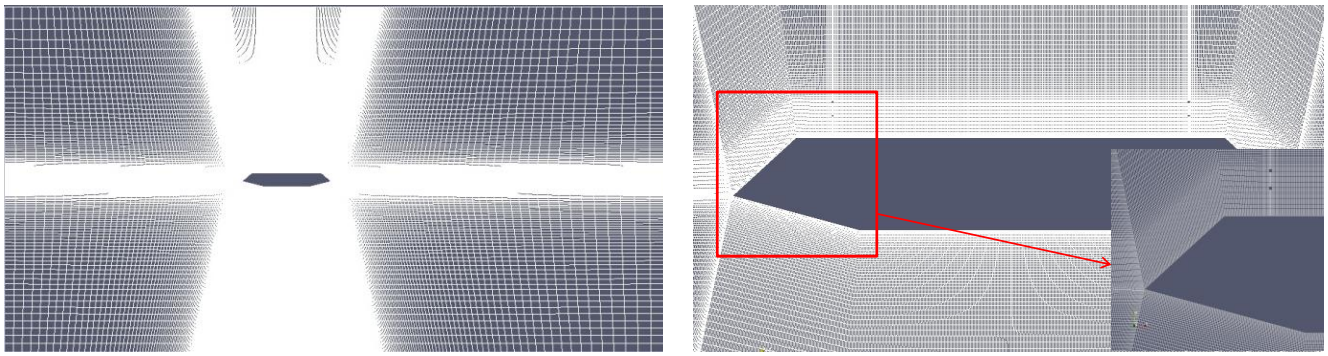

(a) Complete domain (b) Grid near the bridge deck

Fig. 4 Computational grid system adopted for the streamlined bridge deck

3. Validation

The present numerical setup, boundary conditions and grid system were previously validated for a rectangular cylinder of (R of 5) and for a pentagonal shaped bridge deck in Haque *et al*. (2016, 2015b) respectively. In the present study, a new validation study was carried out for rectangular bluff bodies and streamlined bridge deck. First, the performance of the current numerical simulation was checked for predicting the trend in the steady state coefficients and Strouhal number (S_t) due to variation of R from 1 to 8. Then, the surface pressure distribution (C_P) was also validated for a streamlined bridge deck.

Fig. 5 illustrates the influence of R on mean drag (C_D), rms of lift (C_L') and S_t, and compares the current results with past experimental and numerical results. Simulations were carried out at R_{eB} varying from $1.2\text{x}10^4$ to $9.76\text{x}10^4$. The current simulation could reproduce the trend and magnitude quite well. In this test the R was altered and that was also a kind of change in shape and current simulation results had a very good comparison with past results. One point should be noticed that the experimental results are well scattered and the current results lie within the upper or lower bound of past results. For further detailed validation, the mean C_P distribution of a streamlined bridge deck was compared with the experimental result (Šarkić *et al.* 2012). Simulation was conducted for a streamlined bridge deck as mentioned in Šarkić *et al*. (2012) and R_{eB} was set to $1.1\text{x}10^5$. The mean surface pressure distributions are plotted in Fig. 6. Good agreement can be noticed between the experimental and present numerical work. Due to two-dimensional nature of the flow, the current simulation overestimated the pressure value both at the top and bottom surface. It overestimated even larger at the top surface; especially the peak negative pressure at the leading edge corner. However, the overall trend in the pressure distribution was reproduced quite accurately.

4. Influence of width ration and bottom plate slope

To investigate the influence of W and θ_B, the value of W was varied from 1 to 0.3 for four different values and θ_B was varied from 25° to 11° for each of these width ratios as shown in Fig. 7 in details. The top plate slope was maintained arbitrarily at 40°. All the simulations were conducted at a constant R_{eB} and R values of $6.0\text{x}10^4$ and 5, respectively with perforated handrails.

4.1 Steady state force coefficients

The main parameter of interest is the steady state force coefficients. The steady state force coefficients such as drag

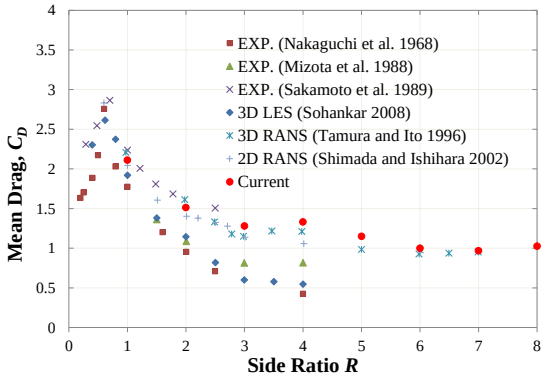

(a) Mean value of drag force coefficient (C_D)

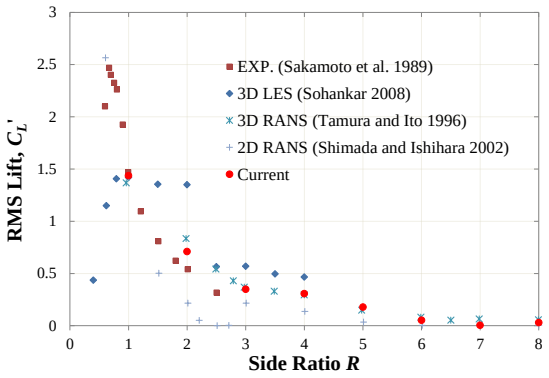

(b) rms value of lift force coefficient (C_L')

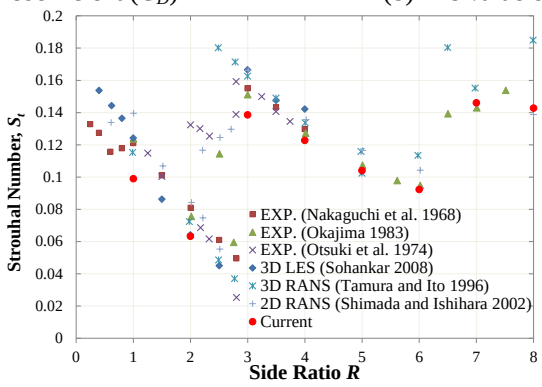

(c) Strouhal number (S_t)

Fig. 5 Influence of R on force coefficients and S_t. Experimental results are: Nakaguchi *et al*. (1968) at R_e=10^5, Sakamoto *et al*. (1989) at R_e=5.5x10^4, Okajima (1983) at R_e=0.42x10^5, Otsuki *et al*. (1974) at R_e=2.2x10^4-5.5x10^5

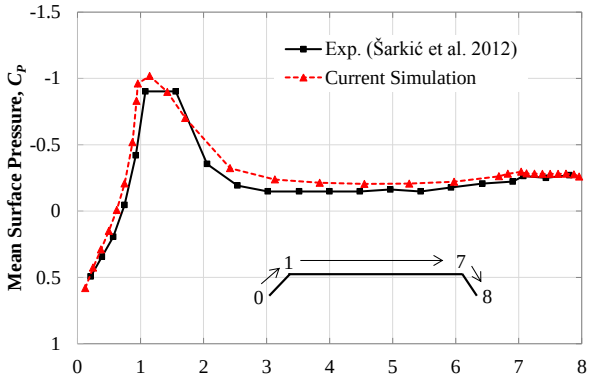

(a) Top surface

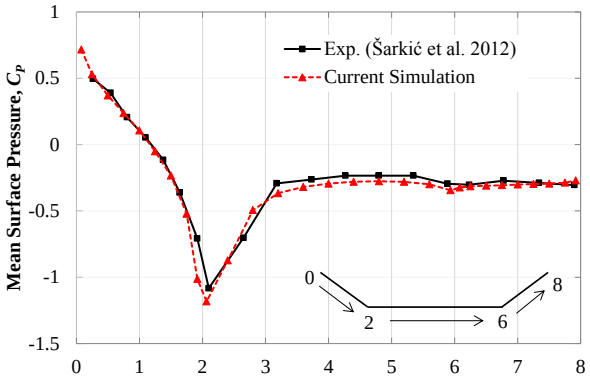

(b) Bottom surface

Fig. 6 Comparison of mean C_P distribution between the present numerical and previous experimental result of Šarkić *et al*. 2012 (R_{eB} at 1.1x10^5)

(C_D), lift (C_L), moment (C_M) and Strouhal number (S_t) are defined as follows

$$C_D = \frac{F_D}{\frac{1}{2}\rho U^2 D} \quad \text{(Downward Positive)} \tag{3}$$

$$C_L = \frac{F_L}{\frac{1}{2}\rho U^2 B} \quad \text{(Upward Positive)} \tag{4}$$

$$C_M = \frac{F_M}{\frac{1}{2}\rho U^2 B^2} \quad \text{(Anti-clockwise Positive)} \tag{5}$$

$$S_t = \frac{fD}{U} \tag{6}$$

where F_D, F_L and F_M are the drag, lift and moment forces acting per unit length on the bridge deck respectively, f is the shedding frequency, B is the top plate width and D is the

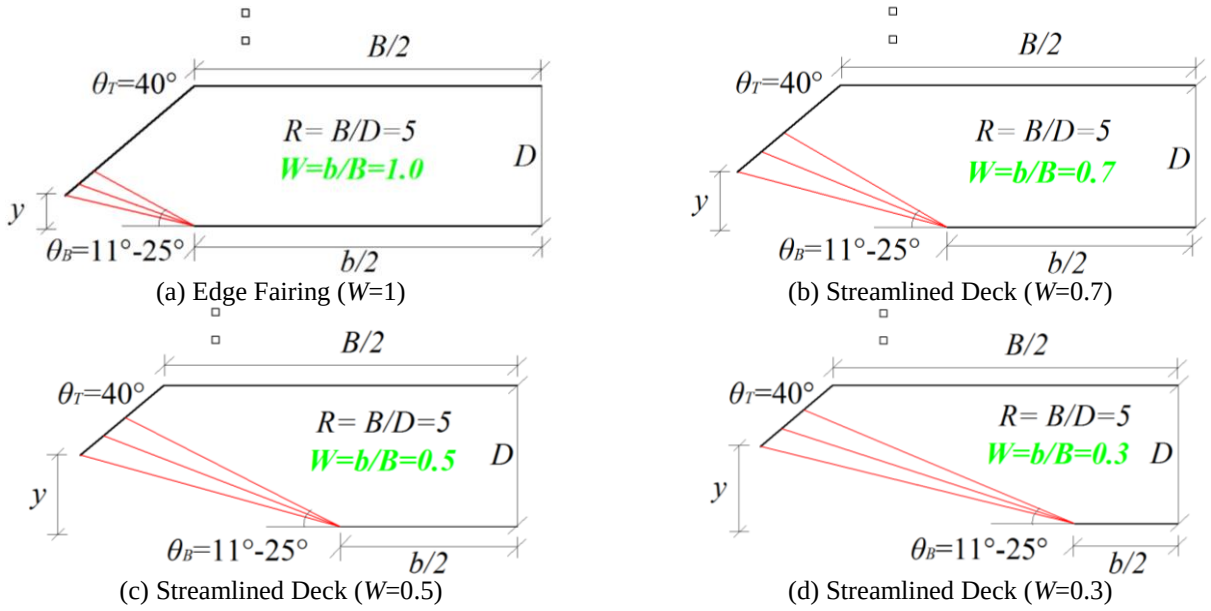

(a) Edge Fairing (W=1) (b) Streamlined Deck (W=0.7)

(c) Streamlined Deck (W=0.5) (d) Streamlined Deck (W=0.3)

Fig. 7 Cross-sectional details of the streamlined decks employed for investigation

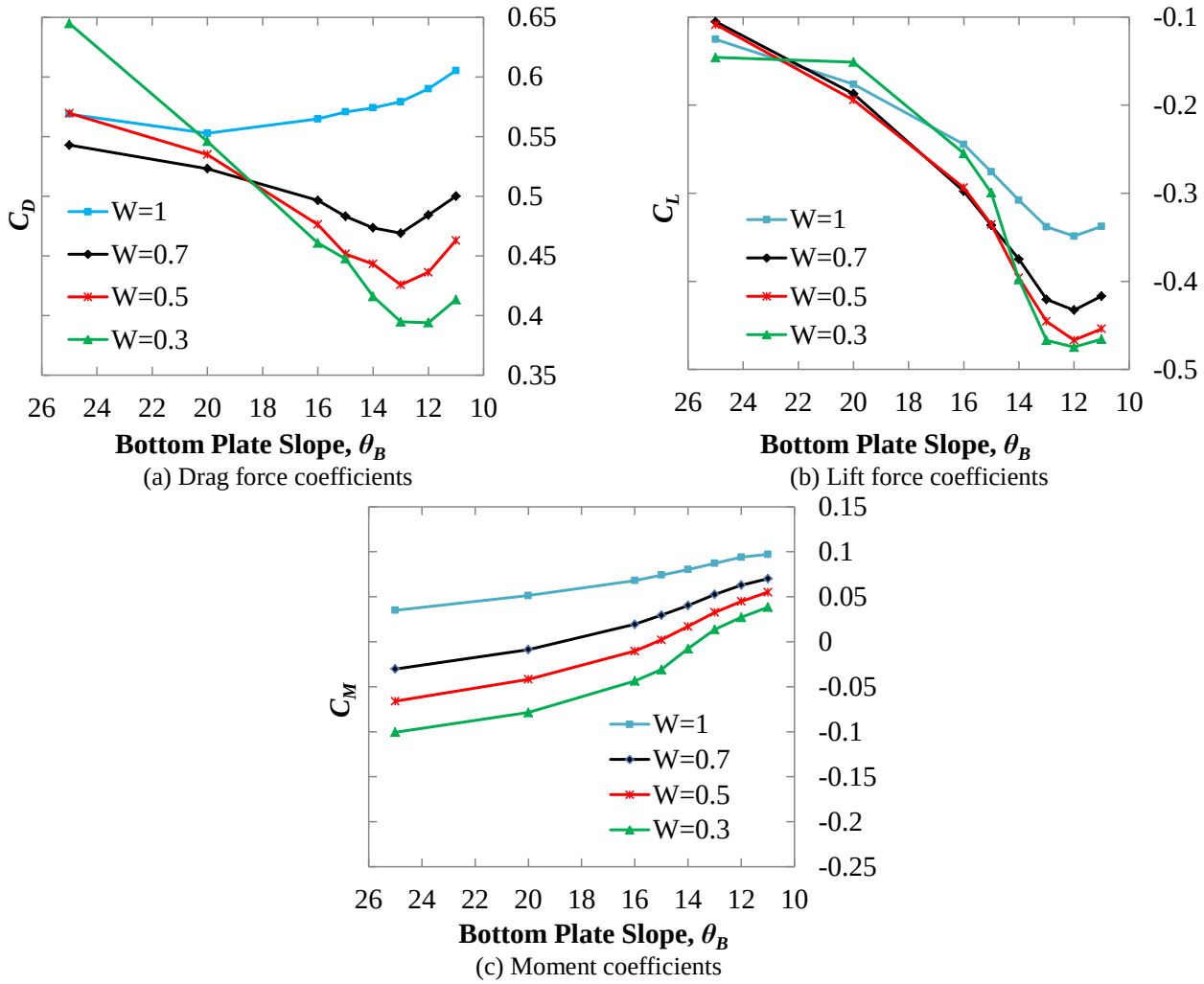

(a) Drag force coefficients (b) Lift force coefficients

(c) Moment coefficients

Fig. 8 Influence of θ_B and W on mean value of steady state force coeffieients

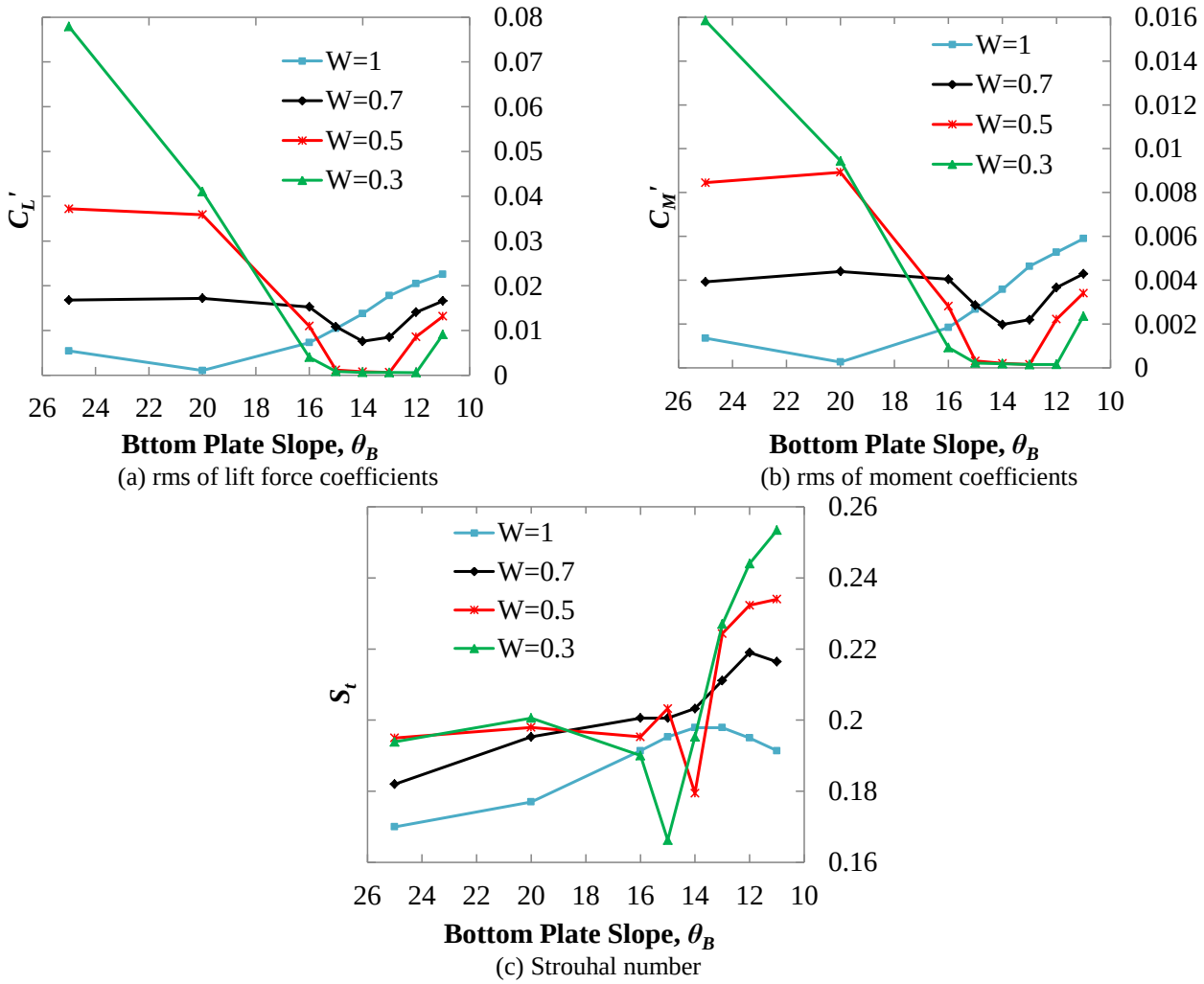

(a) rms of lift force coefficients

(b) rms of moment coefficients

(c) Strouhal number

Fig. 9 Influence of θ_B and W on rms value of steady state force coefficients and S_t

depth of the bridge deck (as shown in Fig. 1). Both the mean and root means square (rms) values of the time varying force coefficients were evaluated. In all the cases, the rms values were calculated from the zero mean force coefficient time histories.

Fig. 8 summarizes the mean steady state force coefficients for various bottom plate slopes and width ratios. The mean value changes a lot both for the θ_B and W. For any value of W, the C_L decreases and C_M increases as the θ_B decreases. On the other hand, for C_D, the minimum C_D value can be obtained at a large bottom plate slope (θ_B=20°) for the large width ratio (W=1), yet for smaller width ratio (W≤0.7) the position of minimum C_D shifts gradually towards smaller θ_B. The sensitivity of the force coefficients increases noticeably as the W decreases. In particular, for small width ratio (W=0.5 or 0.3) the response varies significantly. However, it does not vary so much for large width ratio (W=1). Basically, as the W decreases the l increases and the influence of θ_B on aerodynamic response increases too.

The rms value of C_L and C_M coefficients along with the S_t are plotted in Fig. 9. The rms values of the steady state force coefficients also show similar trend to the results of the mean value of drag (Fig. 8(a)) as discussed earlier. For large bottom plate slope (θ_B =25°-20°) the rms value. increases and for small bottom plate slope (θ_B≤15°) the rms value decreases with the decrease in W. Moreover, as the W decreases much wider range of θ_B yields the least rms value.

However, the S_t does not show any definite trend for large bottom plate slope (θ_B=25°-20°), yet for small bottom plate slope (θ_B≤15°) the S_t increases with the decreases in W. The possible explanation could be as follows. As the W decreases, the shape becomes more streamlined and the shedding frequency (f_v) increases, which increases the S_t. Therefore, in this section we found two distinct zones of θ_B and exhibits similar but opposite trends in results. First one is the large bottom plate slope zone (θ_B =25°-20°) where aerodynamic responses increases as the W decreases. The other one is the small bottom plate slope (θ_B =15°-11°) zone where the aerodynamic responses decreases as the W decreases.

4.2 Surface pressure distribution

Based on previous observation we selected two bottom

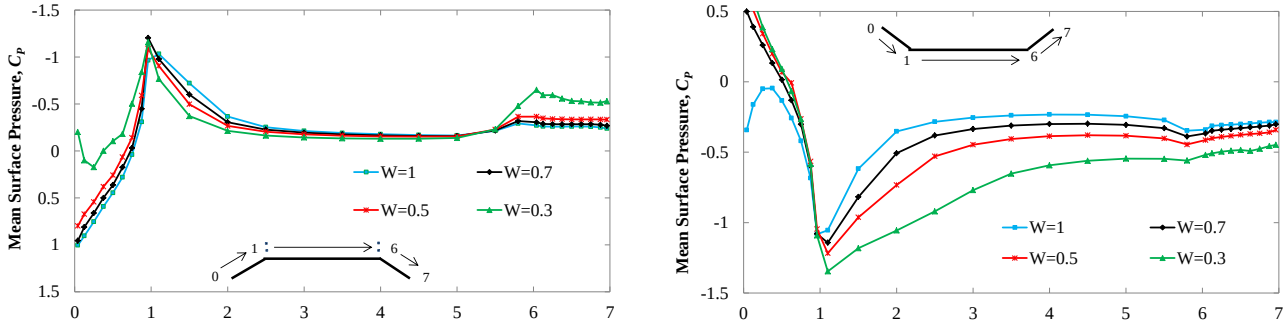

(a) Top surface pressure (b) Bottom surface pressure

Fig. 10 Mean value of surface pressure distribution around the bridge deck with θ_B of 25°

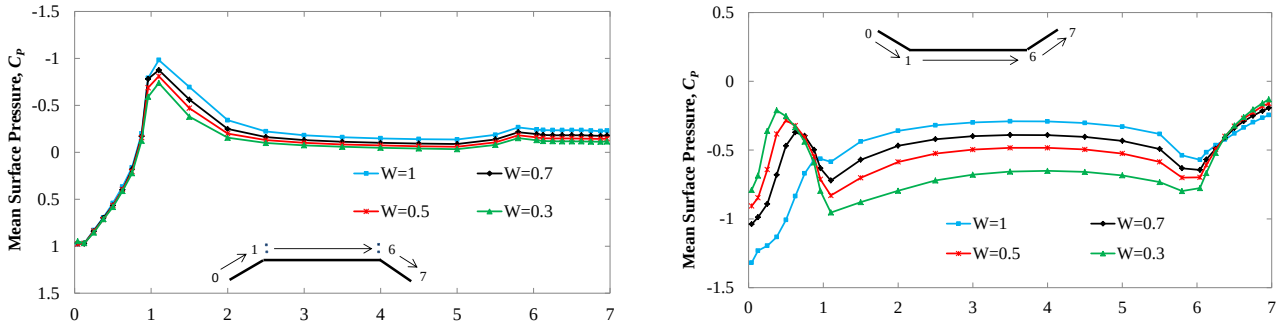

(a) Top surface pressure (b) Bottom surface pressure

Fig. 11 Mean value of surface pressure distribution around the bridge deck with θ_B of 12°

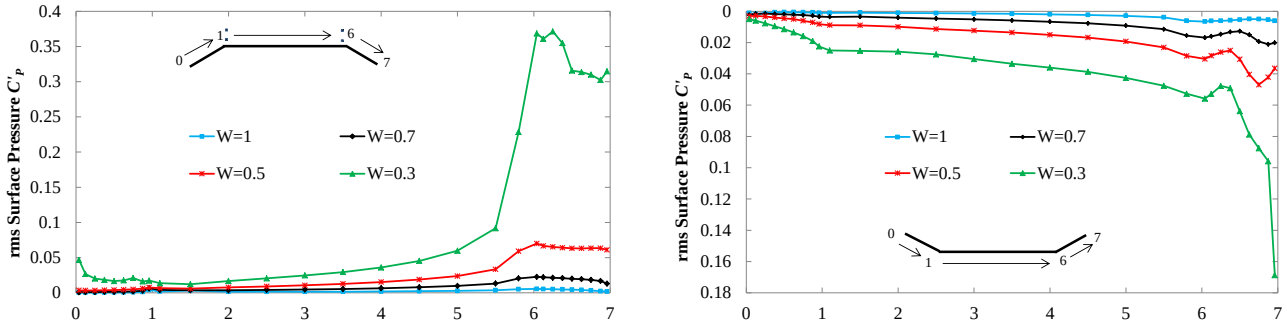

(a) Top surface pressure (b) Bottom surface pressure

Fig. 12 rms value of surface pressure distribution around the bridge deck with θ_B of 25°

plate slopes from two distinct zones : i) θ_B of 25° and ii) θ_B of 12° for detailed pressure field analysis. The surface pressure distributions of bottom plate slope of 25° and 12°are summarized in Figs. 10 and 11, respectively for all four width ratios. Both of these bottom plate slopes (θ_B of 25° and 12°) have similar pressure distribution except variation in magnitude and rather than the top surface, the bottom surface pressure distribution is more influential. The large bottom plate slope (θ_B of 25°) experiences larger suction at the leading edge top and bottom deck surfaces than the small bottom plate slope (θ_B of 12°). Based on Figs. 10 and 11, the lift characteristics we found in Fig. 8(b) can be explained well. For any value of bottom pate slope (θ_B of 25° and 12°), as the W decreases the bottom deck suction increases dramatically due to faster movement of the flow and increases the negative lift value. Further, in case of small bottom plate slope (θ_B of 12°), smaller pressure recoveries occur at the bottom deck trailing edge side as compared to the large bottom plate slope. It results in higher negative lift for small bottom plate slope (θ_B of 12°) than the large bottom plate slope (θ_B of 25°).

The rms values of surface pressure distributions are the rms value of surface pressure distributions are plotted in Figs. 12 and 13 for bottom plate slopes of 25° and 12°, respectively. The rms value of pressure also shows the similar characteristics we found in Figs. 9(a) and 9(b) for large (θ_B of 25°) and small (θ_B of 12°) bottom plate slopes in relation to the W, respectively. Large rms value can be

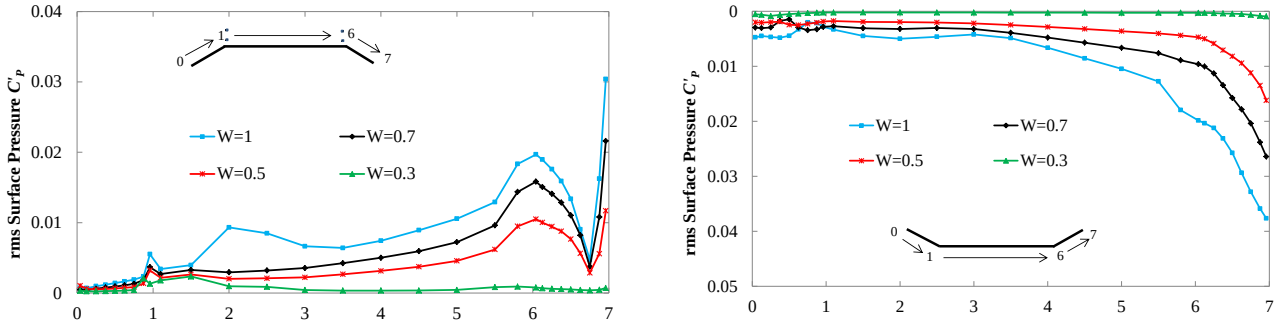

(a) Top surface pressure (b) Bottom surface pressure

Fig. 13 rms value of surface pressure distribution around the bridge deck with θ_B of 12°

observed at the trailing edge side. After close scrutiny we found that the after-body vortex shedding activity is the main cause of those large fluctuations of pressure at the trailing edge side. In the following section both the velocity and vorticity fields around the bridge decks were analyzed to better understand the flow mechanism in relation to the geometric configuration.

4.3 Velocity distribution

The time averaged velocity distribution for θ_B of 25° and 12° are plotted in Fig. 14 for the selected *W*. For all of these sections, flow separation can be noticed at the leading and the trailing edge side. However, the trailing edge side flow separation governs over the leading edge side. In case of large bottom plate slope (θ_B of 25°) the bottom surface trailing edge separation is pronounced and increases as the *W* decreases. On the other hand, for small bottom slope (θ_B of 12°) there is no trailing edge separation at the bottom surface trailing edge. For small bottom plate slope (θ_B of 12°) the top surface trailing edge separation is crucial. However, as the *W* decreases the top surface trailing edge separation gradually decreases.

Based on this observation we can explain the trend in the results we obtained previously for drag (Fig. 8(a)) and rms values (Figs. 9(a) and 9(b)). For large bottom plate slope (θ_B of 25°) as the *W* decreases the nose (*y/D*) of the fairing goes up and the bottom surface trailing edge separation increases which increases the wake size and vortex activity. Therefore, for large bottom plate slope (θ_B of 25°) the drag and rms value of steady state force coefficients increases with the decrease in *W*.

Similarly, for small bottom plate slope (θ_B of 12°) as the *W* decreases the nose (*y/D*) of the fairing also goes up which decreases the top surface trailing separation without any bottom surface trailing edge separation. As a result the wake becomes smaller at smaller *W* which decreases the drag and rms value of the force coefficients. However, for the θ_B of 12°, a *W* of 0.3 is required to obtain the least rms response (see Figs. 9(a) and 9(b)) so that the nose height (*y/D*) becomes high enough and the top surface wake becomes less influential. Therefore, there must be some margins of nose height, if the nose goes above that height the top surface wake becomes small and vortex becomes less influential when there is no trailing edge separation.

The vorticity distribution around the bridge deck is shown in Fig. 15 for θ_B of 14° and 12°. The nose locations (*y/D*) are indicated at the title of the corresponding figures. As can be seen for θ_B of 14° no clear after-body vortex activity can be noticed when the *y/D* value reaches to 0.47 for the *W* of 0.5. However, for the same *W* the bottom plate slope of 12° having the *y/D* of 0.42 still shows clear after-body vortices. As the width ratio decreases further (*W*=0.3), the *y/D* increases to a value of 0.51 and then the after-body vortex activity weakens. Therefore, we can presume that for smaller bottom plate slope ($\theta_B \leq 15°$) and the shapes without having bottom surface trailing edge separation, nose should be tried to place at least on the upper half ($y/D \geq 0.5$) of the deck to obtain smaller aerodynamic forces and to reduce the after-body vortex activity.

5. Influence of side ratio

All previous simulations were conducted for a *R* value of 5 and we got some trends in the results. It is important to explore whether the trends in the result alter depending on the *R* or not. One new set of simulation was conducted for the bridge deck with a *R* of 8 and *W* of 0.55. The θ_T was set to 40° and the θ_B was varied from 25° to 11° similar to the previous cases. The same inlet velocity similar to the last section was used to make the comparison feasible.

Fig. 16 presents the most relevant force coefficients of the bridge deck with the *R* of 5 and 8. Similarity was maintained in terms of *W* of 0.5. As can be seen from the figure the trend in the results remains almost unchanged when the *R* alters from 5 to 8 for the same value of *W*. It should be also noted that even though the width ratio was the same we could not maintain similarities in terms of *y/D*. However, as we can see from the figure the variation of the nose location does not affect the trend in the results significantly. Fig. 17 compares the time averaged velocity field around the bridge decks for a θ_B of 14°. The bridge deck with *R* of 8 possesses a bit smaller wake as compared to the *R* of 5 due to increase in *y/D* value with lesser separation at the trailing edge, yet the overall flow behavior is quite similar.

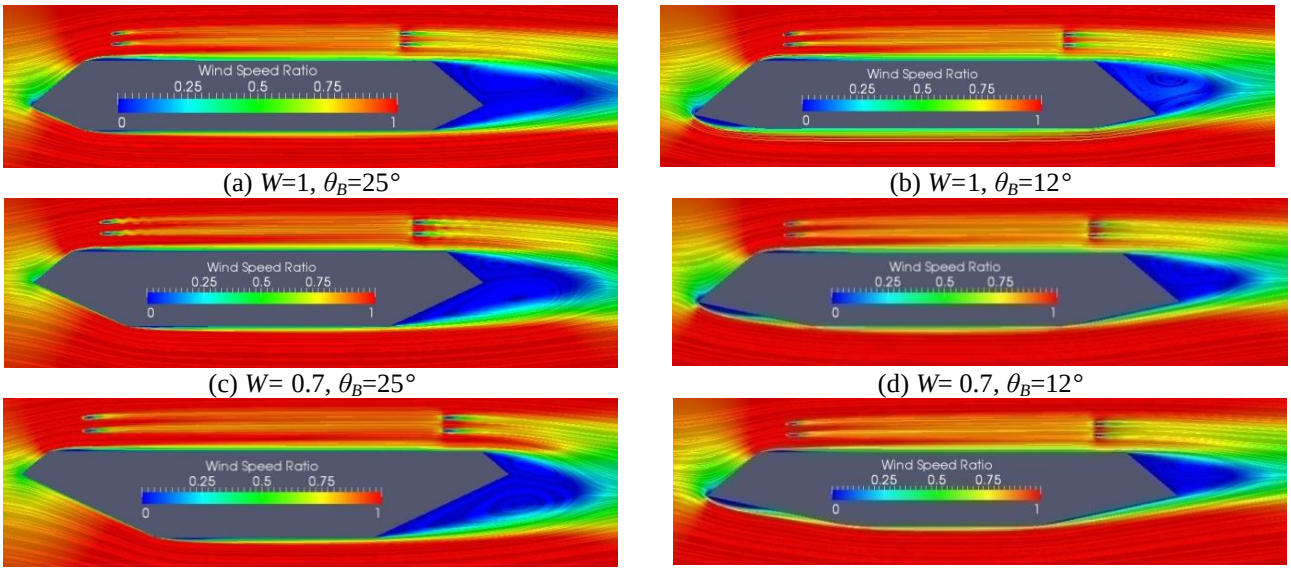

(a) W=1, θ_B=25° (b) W=1, θ_B=12°

(c) W= 0.7, θ_B=25° (d) W= 0.7, θ_B=12°

(e) W= 0.5, θ_B=25° (f) W= 0.5, θ_B=12°

Fig. 14 Comparison of time averaged velocity distributions (normalized with the inlet velocity) around the bridge decks for θ_B of 25° and 12°

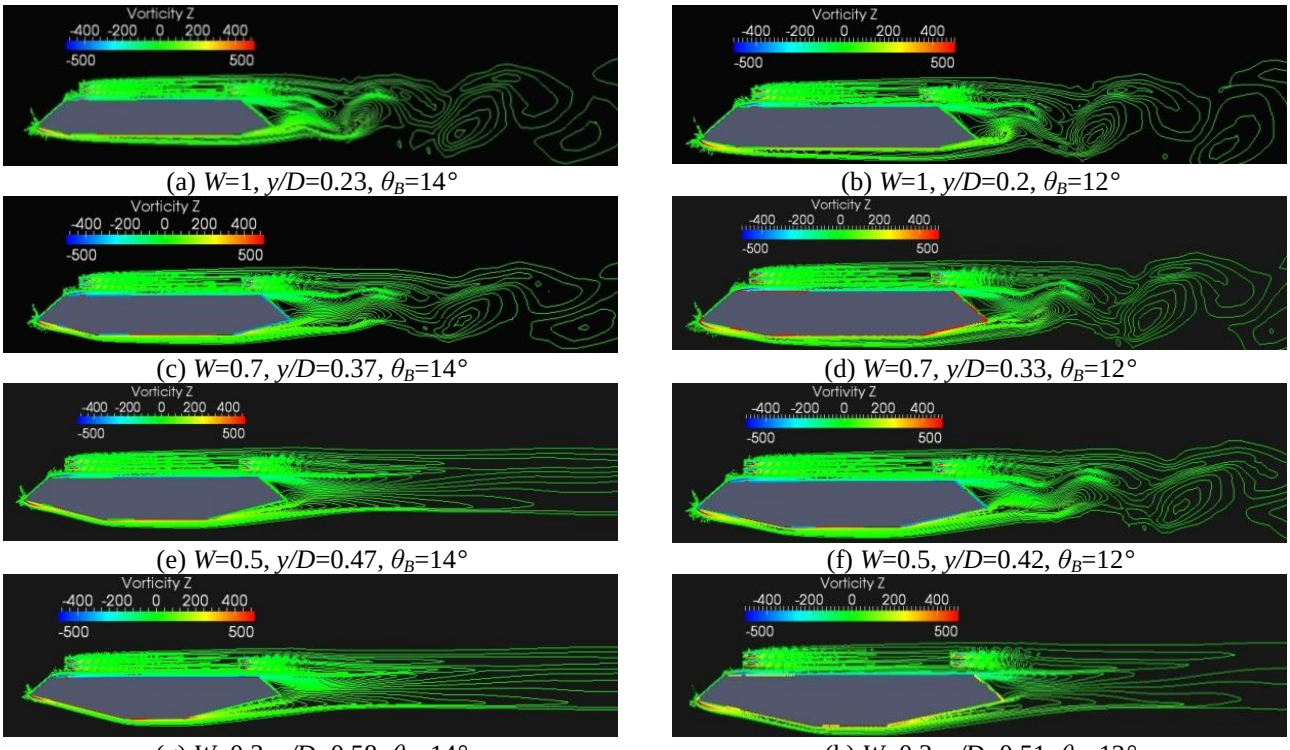

(a) W=1, y/D=0.23, θ_B=14° (b) W=1, y/D=0.2, θ_B=12°

(c) W=0.7, y/D=0.37, θ_B=14° (d) W=0.7, y/D=0.33, θ_B=12°

(e) W=0.5, y/D=0.47, θ_B=14° (f) W=0.5, y/D=0.42, θ_B=12°

(g) W=0.3, y/D=0.58, θ_B=14° (h) W=0.3, y/D=0.51, θ_B=12°

Fig. 15 Comparison of Vorticity plot around bridge deck for bottom plate slopes (θ_B) of 14° and 12°

6. Influence of reynolds number

In the last two sections we explored the influence of various shaping parameters on aerodynamic responses and flow field for a constant inlet velocity. In this section, we present the influence of Reynolds number for a bridge deck with a R of 5, W of 0.7 and θ_B of 14°. The main intention was to check the trend in the results and flow field due to variation of R_{eB}. The R_{eB} was varied from $1.65\text{x}10^4$ to $25\text{x}10^4$. Due to expensive nature of the simulation, the maximum R_{eB} was limited to $25\text{x}10^4$. Total 87,659 and 775,267 numbers of elements were used to discretize the flow for R_{eB} of $1.65\text{x}10^4$ and $25\text{x}10^4$ respectively.

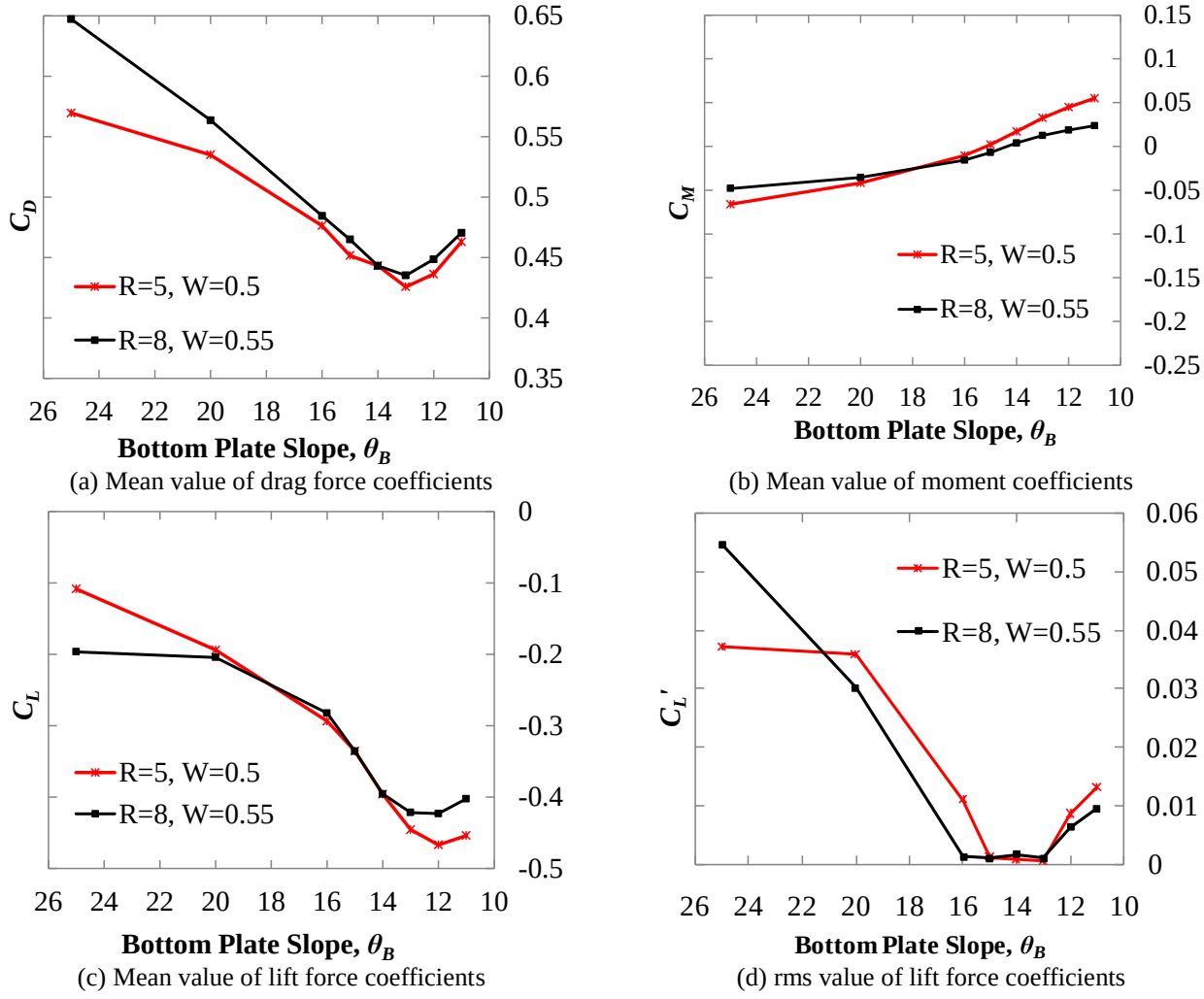

(a) Mean value of drag force coefficients

(b) Mean value of moment coefficients

(c) Mean value of lift force coefficients

(d) rms value of lift force coefficients

Fig. 16 Influence of R on steady state force coefficients

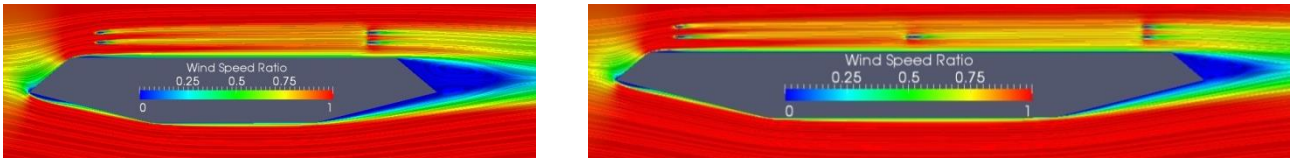

(a) R=5, W=0.5

(b) R=8, W=0.55

Fig. 17 Comparison of time averaged velocity distribution (normalized with the inlet velocity) around the bridge deck for R of 5 and 8 with a θ_B of 14°

Fig. 18 plots the mean and rms value of steady state force coefficients versus the R_{eB}. The mean value of the force coefficients become almost R_{eB} independent beyond a value of 13.0x10^4. The mean value of C_D decreases with the increase in R_{eB}. Similar trend was also found by Schewe and Larsen (1998) and Schewe (2001) where R_{eB} effect was investigated for a bluff bridge deck section. Both the negative C_L and the mean C_M increase with the increase in R_{eB}. Similarly to mean value of the coefficients, the rms value of all the coefficients and S_t increase significantly as the R_{eB} increases. Therefore, the results we presented in the last two sections have R_{eB} effects. However, we mainly made relative comparison among the aerodynamic responses of the bridge deck due to variation of shaping parameters and discussion was limited to the trend in the results. At high Reynolds number (R_{eB}≥13x10^4) the magnitude of response will change, yet the trend in the result should not alter significantly as discussed here and previously (Schewe and Larsen 1998, Schewe 2001) that with the increase in R_{eB} the response shows definite pattern in the results. Even so, depending on the shape of the bridge deck the R_{eB} effect may vary but that should not be significant as all of them are streamlined in shape and the θ_B were varied only for 25°-11°.

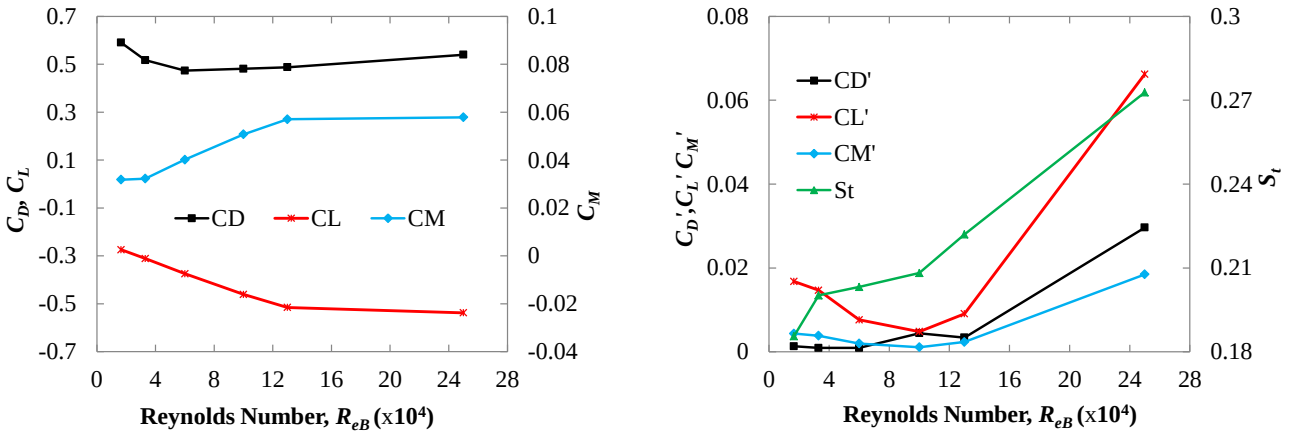

(a) Mean value (b) rms value

Fig. 18 Effects of R_{eB} on mean and rms value of steady state force coefficients for the deck with a θ_B of 14°, R=5 and W=0.7

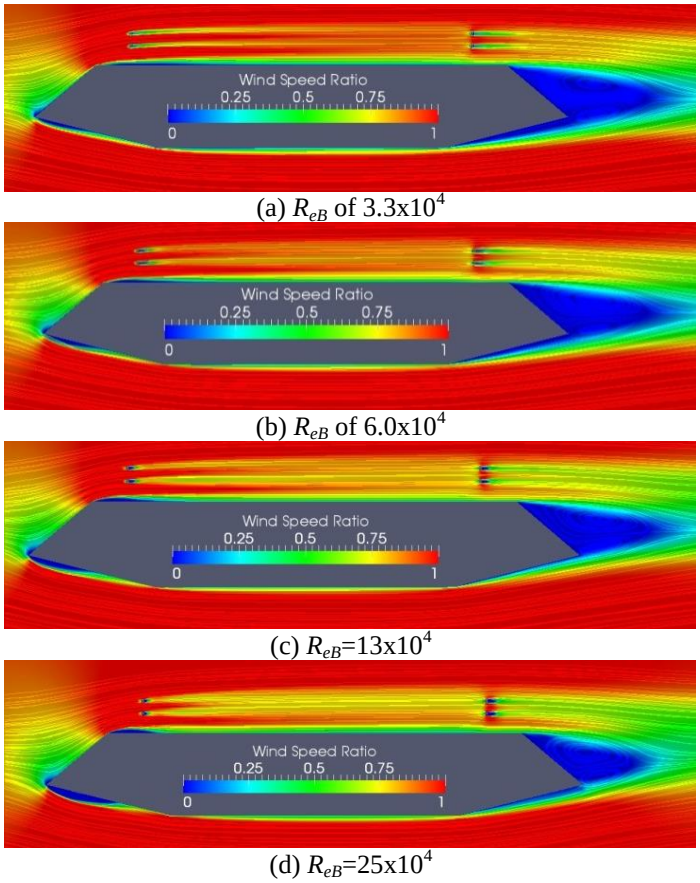

(a) R_{eB} of 3.3x10^4

(b) R_{eB} of 6.0x10^4

(c) R_{eB}=13x10^4

(d) R_{eB}=25x10^4

Fig. 19 Reynolds number effects on time averaged velocity field (normalized with the inlet velocity) for a θ_B of 14°, R=5 and W=0.7

To understand the trend in mean value of steady state force coefficients, the time averaged velocity distributions are plotted for four Reynolds number values in Fig. 19. Figure 19 shows that the bottom surface leading and the trailing edges are mostly affected due to increase in R_{eB}. As the R_{eB} increases the bottom surface leading edge separation increases and increases the suction and negative lift value. However, the separation at the bottom deck trailing edge side decreases and stops completely when the R_{eB} reaches to value of 13x10^4. As a result, the wake becomes smaller and the drag value decreases with the increase in R_{eB}. Similar trend for trailing edge separation was also noticed by Schewe and Larsen (1998) and Schewe (2001). However, the amount of separation was quite large as the section had

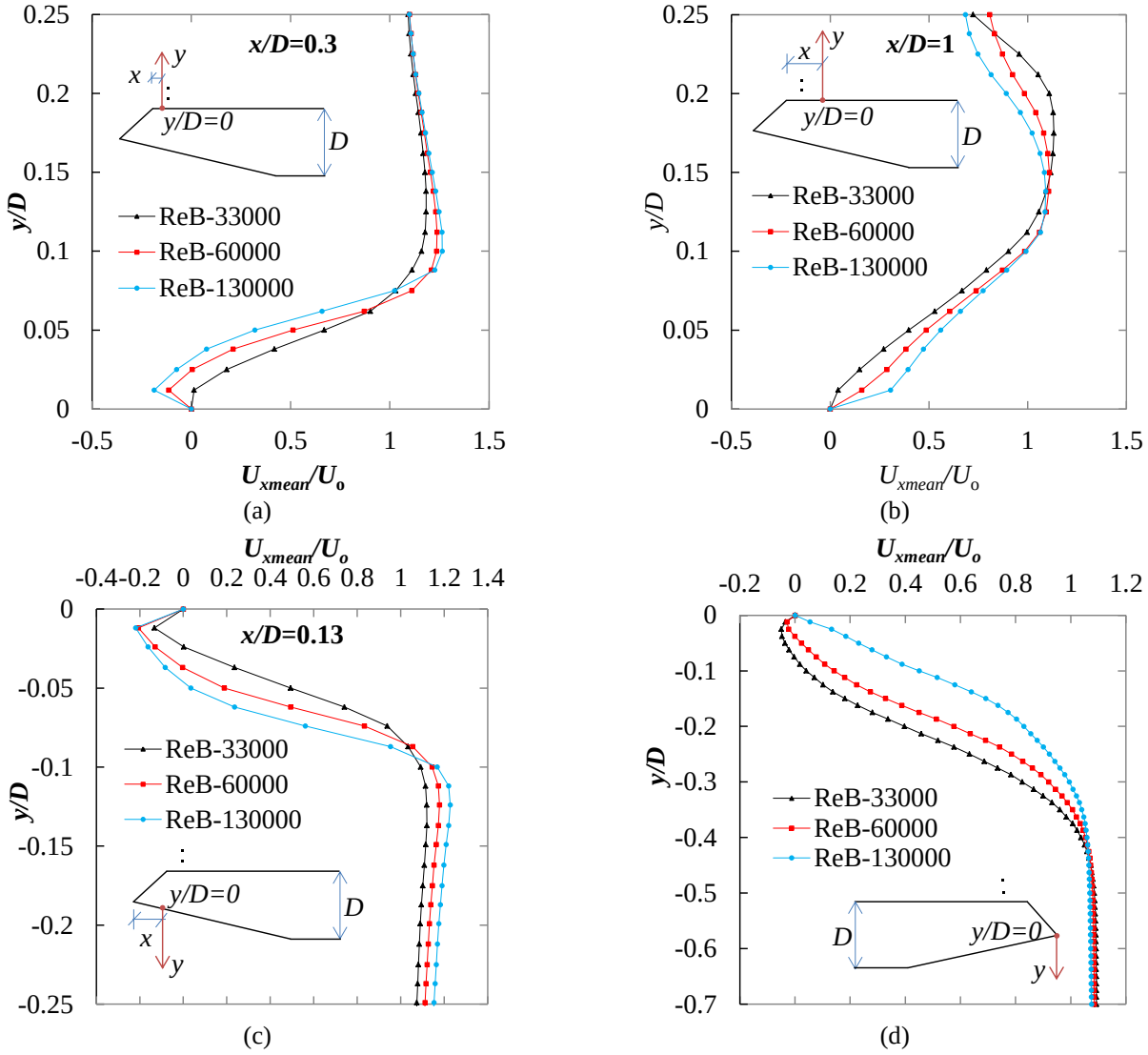

Fig. 20 Reynolds number (R_{eB}) effects on vertical plane velocty distribtion at various location around the bridge deck

very large value of θ_B. Moreover, in their section the leading separation appeared at bottom surface corner toe near the horizontal plate while for the present streamlined section the separation shifts just near the nose of the leading edge fairing. At the top surface leading edge side, the R_{eB} increased the flow reattachment tendency similarly to past experimental work (Schewe 2001), yet the flow separation at the leading edge corner increased with the increase in R_{eB}. To show the influence of R_{eB} on various flow features more clearly, the vertical plane velocity distributions are summarized in Fig. 20. The figure reflects the effects of R_{eB} on flow field quantitatively as discussed earlier.

7. Conclusions

Influence of various shaping parameters such as the bottom plate slope (θ_B), width ratio (W) and side ratio (R) were investigated on the aerodynamic response of a streamlined bridge deck. Reynolds number (R_{eB}) was altered up to a reasonable range to observe the trend in the response and the flow field due to variation of R_{eB}. The findings of the present study are summarized below:

1. The influence and effectiveness of θ_B depends on the newly defined shaping parameter W. As the W decreases the deck becomes more streamlined and the influence of θ_B increases on aerodynamic response. The variation of W and θ_B control the nose height (y/D) of the fairing and y/D has direct influence on the after-body vortex activity.
2. Large bottom plate slopes ($\theta_B \approx 20°$) exhibit better aerodynamic performance for the bride deck with large width ratio ($W \approx 1$) as the wake size remains comparatively small with lesser vortex activity. Small bottom plate slopes ($\theta_B \leq 15°$) does not work well for large width ratio ($W \approx 1$). If the small bottom plate slopes ($\theta_B \leq 15°$) are adopted the trailing edge flow separation stops, yet the nose of the fairing moves downward and large vortex forms on the trailing edge

top surface of the deck as a result the aerodynamic performance deteriorates. Therefore, for large width ratio (W≈1) bridges, large bottom plate slopes (θ_B≈20°) can be adopted.

3. For the bridge deck with smaller width ratio (W≈0.5), small bottom plate slopes (θ_B≤15°) shows better aerodynamic responses. When small bottom plate slopes (θ_B≤15°) are chosen, the trailing edge flow separation stops that lefts no provision for formation of vortex at the trailing edge bottom surface and due to smaller width ratio (W≈0.5), the nose of the fairing goes upward that decreases the size of the vortex forms on the tailing edge top surface. The size of the wake and vortex strength reduces significantly when the nose of the fairing is placed on the upper half (y/D≥0.5) of the deck for any value of θ_B smaller than 15°. Therefore, a small bottom plate slopes (θ_B≤15°) with higher nose location (y/D≥0.5) can be a better choice for shaping long-span bridge decks and that is mainly achievable for the small width ratio (W≈0.5) bridge decks.
4. The value of R did not alter the trend in the results due to variation of θ_B. The deck with large side ratio (R=8) had almost similar aerodynamic response to the small side ratio (R=5) when a similarity in width ratio (W) was maintained. However, the variation of R_{eB} altered the aerodynamic responses noticeably. The increase in R_{eB} increases the bottom surface leading edge separation and decreases the trailing edge separation that increases the negative lift value and decreases the drag. For this type of streamlined bridge deck aerodynamic analysis may be carried out at a R_{eB} higher than a value of $13x10^4$ to obtain Reynolds number independent results.

In the present study, the aerodynamic responses were predicted by means of properly validated URANS simulation and some useful findings were obtained. However, further experimental studies and simulations using other CFD techniques such as LES are required to reconfirm the conclusions presented before practical application.

References

Brusiani, F., De Miranda, S., Patruno, L., Ubertini, F. and Vaona, P. (2013), "On the evaluation of bridge deck flutter derivatives using RANS turbulence model", *J. Wind Eng. Ind. Aerod.*, **119**, 39-47.

De Miranda, M. and Bartoli, G. (2001), "Aerodynamic optimization of decks of cable-stayed bridges. Cable-Supported Bridges – Challenging Technical Limits", *Proceeding of the IABSE Conference*, Seoul Korea, 12-14 June.

Franke, J., Hirsch, C., Jensen, A.G., Krüs, H.W., Schatzmann, M., Westbury, P.S., Miles, S.D., Wisse, J.A. and Wright, N.G. (2004), "Recommendations on the use of CFD in wind engineering", (Ed., van Beeck, J.P.A.J.), *Proceedings of the International Conference on Urban Wind Engineering and Building Aerodynamics.* COST Action C14, Impact of Wind and Storm on City Life Built Environment. Von Karman Institute, Sint-Genesius-Rode, Belgium, 5-7 May.

Fujino, Y. and Siringoringo, D. (2013), "Vibration mechanisms and controls of long-span bridges: A review", *Struct. Eng., IABSE*, **23**(3), 248-268.

Haque, M.N., Katsuchi, H., Yamada, H. and Nishio, M. (2014), "Investigation of bridge deck shaping effects on aerodynamic response by rans simulation", *In Proceedings of International Symposium on the Computational Wind Engineering*, June 8-12, Hamburg University, Hamburg, Germany.

Haque, M.N., Katsuchi, H., Yamada, H. and Nishio, M. (2015a), "A numerical study on aerodynamics of a pentagonal shaped cable-supported bridge deck", *J. Struct. Eng. (JSCE)*, **61A**, 375-387.

Haque, M.N., Katsuchi, H., Yamada, H. and Nishio, M. (2015b), "Flow field analysis of a pentagonal-shaped bridge deck by unsteady RANS", *Eng. Appl. Comput. Fluid Mech.*, **10**(1), 1-16.

Haque, M.N., Katsuchi, H., Yamada, H. and Nishio, M. (2015c), "Strategy to develop efficient grid system for flow analysis around two-dimensional bluff bodies", *J. Civil Eng.- KSCE*, **20**(5), 1-12.

Haque, M.N., Katsuchi, H., Yamada, H. and Nishio, M. (2016), "Investigation of edge fairing shaping effects on aerodynamic response of long-span bridge deck by unsteady RANS" *Arch. Civil Mech. Eng.*, **16**(4), 888-900.

Kawatani, M., Kim, J., Uejima, H. and Kobayashi, H. (1993), "Effects of turbulent on vortex-induced oscillation of bridge girders with basic sections", *J. Wind Eng. Ind. Aerod.*, **49**, 477-486.

Kelkar, K.M. and Patankar, S.V. (1992), "Numerical prediction of vortex shedding behind a square cylinder", *Int. J. Numer. Meth. Fl.*, **14**(03), 327.

Larsen, A. (1993), "Aerodynamic aspects of the final design of the 1624m suspension bridge across the great belt", *J. Wind Eng. Ind. Aerod.*, **48**, 261-285.

Larsen, A. and Wall, A. (2012), "Shaping of bridge girders to avoid vortex shedding response", *J. Wind Eng. Ind. Aerod.*, **104-106**, 159-165.

Menter, F. and Esch, T. (2001), "Elements of industrial heat transfer prediction", *Proceedings of the 16th Brazilian Congress of Mechanical Engineering*.

Menter, F.R. (1993), "Zonal two-equation k–ω turbulence models for aerodynamic flows", *AIAA paper*, **93**, 2906.

Miranda, S.D., Patruno, L., Ubertini, F. and Vairo, G. (2014), "On the identifications of the flutter derivatives of bridge deck via RANS turbulence models: Benchmarking on rectangular prisms", *Eng. Struct.*, **76**, 359-370.

Mizota, T., Yamada, H., Kubo, Y., Okajima, A., Knisely, C.W. and Shirato, H. (1988), "Aerodynamic characteristics of fundamental structures, part 1, section 2", *J. Wind Eng.*, **36**, 50-52 (in Japanese).

Nagao, F., Utsunomiya, H., Oryu, T. and Manabe, S. (1993), "Aerodynamic efficiency of triangular fairing on box girder bridge", *J. Wind Eng. Ind. Aerod.*, **49**, 565-574.

Nakaguchi, H., Hashimoto, K. and Muto, S. (1968), "An experimental study on aerodynamic drag of rectangular cylinders", *J. Japan Soc. Aeronaut. Space Sci*., **16**, 1-5.

Okajima, A. (1983), "Flow around a rectangular cylinder with a section of various width/height ratios", *J. Wind Eng.*, **17**, 1-19.

Otsuki, Y., Washizu, K., Tomizawa, H. and Ohya, A. (1974), "A note on the aeroelastic instability of a prismatic bar with square section", *J. Sound Vib*., **34**(2), 233-248.

Patruno, L. (2015), "Accuracy of numerically evaluated flutter derivatives of bridge deck sections using RANS: Effects on the flutter onset velocity", *Eng. Struct.*, **89**, 49-65.

Sakai, Y., Ogawa, K., Shimodoi, H. and Saitoh, T. (1993), "An experimental study on aerodynamic improvements for edge girder bridges", *J. Wind Eng. Ind. Aerod.*, **49**, 459-466.

Sakamoto, H., Haniu, H. and Kobayashi, Y. (1989), "Fluctuating

force acting on rectangular cylinders in uniform flow on rectangular cylinders with fully separated flow", *T. Japan Soc. Mech. Engineers, Series B*, **55**(516) 2310-2317.

Šarkić, A., Fisch, R., Höffer, R. and Bletzinger, K. (2012), "Bridge flutter derivatives based on computed, validated pressure fields", *J. Wind Eng. Ind. Aerod.*, **104-106**, 141-151.

Schewe, G. (2001), "Reynolds-number effects in flow around more-or-less bluff bodies", *J. Wind Eng. Ind. Aerod.*, **89**, 1267-1289.

Schewe, G. and Larsen, A. (1998), "Reynolds number effects in the flow around a bluff bridge deck cross section", *J. Wind Eng. Ind. Aerod.*, **74-76**, 829-838.

Shimada, K. and Ishihara. T. (2002), "Application of a modified k–e model to the prediction of aerodynamic characteristics of rectangular cross-section cylinders", *J. Fluid. Struct.*, **16**, 465-485.

Sohankar, A. (2008), "Large Eddy Simulation of flow past rectangular-section cylinder : Side ratio effects", *J. Wind Eng. Ind. Aerod.*, **96**, 640-655.

Sohankar, A., Davidson, L. and Norberg, C. (1995), "Numerical simulation of unsteady flow around a square two-dimensional cylinder", *Proceeding of 12th Australasian Fluid Mechanics Conference*, 10-15 December, Sydney, Australia.

Sohankar, A., Davidson, L. and Norberg, C. (1998), "Low-Reynolds- number flow around a square cylinder at incidence: study of blockage, onset of vortex shedding and outlet boundary condition", *Int. J. Numer. Meth. Fl.*, **26**, 39-56.

Sukamta, Nagao, F., Noda, M. and Muneta, K. (2008), "Aerodynamic stabilizing mechanism of a cable stayed bridge with two edge box girder", *Proceedings of the 6th International Colloquium on Bluff Body Aerodynamics and Applications*, Milano, Italy, 20-24 July.

Tamura, T. and Ito, Y. (1996), "Aerodynamic characteristics and flow structures around a rectangular cylinder with a section of various depth/breadth ratios", *J. Struct. Constr. Eng. (Transactions of Architectural Institute of Japan)*, **486,** 153-162.

Wang, Q., Liao, H., Li, M. and Xian, R. (2009), "Wind tunnel study on aerodynamic optimization of suspension bridge deck based on flutter stability", *Proceedings of the 7th Asia-Pacific Conference on Wind Engineering*, November, 8-12, Taiwan.

Yamaguchi, K., Suzuki, S., Kitahara, T., Takeuci, T., Miyazaki, M. and Kazama, K. (1986), "Effects of venting and fairing on vortex-induced oscillations and flutter of box bridge deck", *Proceedings of the National Symposium on Wind Engineering*, (Japanese).

CC